1
PV Models

1.1 Introduction

As for any physical system, PV cell modeling can be done with different levels of accuracy, depending on the user's purposes. In this book the PV generator is always modeled through an equivalent circuit and by using concentrated parameters and variables. Indeed, the aim is to give the reader tools for implementing the PV array model in simulation environments, allowing them to analyze and design the whole PV generator, including the power-processing system feeding a load or the grid. For users interested in this kind of study, access to data concerning the physical properties of the semiconductor material involved or parameter values that depend on the cells' manufacture, such as dopant concentrations or material response to the radiation spectrum, is either not easy or the figures are not readily translated into circuit parameters. Instead, the use of laboratory measurements at the PV terminals, in terms of current and voltage values, or use of experimental data from the product datasheet, are more viable ways of proceeding.

This chapter introduces the two main circuit PV models used in the literature: the single-diode and the double-diode models. The first is the more widely used because of the reduced number of circuit parameters to be identified. The double-diode model (DDM) has better accuracy, especially at low irradiance levels, but it requires a more involved identification of the parameter values. Thus while some space is dedicated in this chapter to the DDM, in the following chapters the single-diode model (SDM) will be considered the reference one.

1.2 Modeling: Granularity and Accuracy

In the last five years a huge literature has been devoted to modeling PV sources, for two main purposes. The first is the reproduction of the I–V curve at the generator terminals through a suitable electrical model, regardless of the size of the PV source: from one PV cell, or even sub-portions of it, up to large PV fields made of series-connected modules forming strings that are in turn connected in parallel. The second purpose is performing energetic analyses concerning plant productivity, using models based on empirical or semi-empirical equations.

The first set of models aims to describe the functional current–voltage relationship at the PV terminals on the basis of the equivalent electrical circuit of the PV source.

Photovoltaic Sources Modeling, First Edition. Giovanni Petrone, Carlos Andrés Ramos-Paja and Giovanni Spagnuolo.

Companion Website: www.wiley.com/go/petrone/Photovoltaic_Sources_Modeling

Such models are usually scalable and the parameter values can be varied according to the operational weather conditions at the PV source. They are also useful for modeling unusual operating conditions, such as mismatches due to partial-shading phenomena. The implementation in circuit-oriented simulators such as PSPICE and PSIM, or in general-purpose simulation environments such as MATLAB® and SCILAB, is almost straightforward. This allows study of the PV source together with dedicated controls, power-processing systems, switching converters, and so on. The PV-source non-linearity is accurately reproduced by these models, but at the cost of a significant computational burden, especially if the granularity of the simulation is at the cell, or even sub-cell level, in the context of a large PV field consisting of thousands of cells. As a consequence, PV equivalent circuit models allow simulations of systems to be performed over short time windows, usually of fractions of a minute.

The second set of models is aimed at performing long-term analyses – over days or months – and they therefore cannot use detailed descriptions of the current–voltage relationship in any operating conditions. Instead, they use simplified equations in which the energy produced by the PV source is described as a function of the environmental conditions and parameters related to the installation type. These approaches usually require tuning, with correcting factors based on experimental measurements used to account for the real operating conditions of the PV field. Approaches based on fuzzy logic [1] and neural networks [2] are often used to take into account the historical meteorological data of the installation site when estimating the produced energy, in order to predict the pay-back time and to evaluate the economic viability of the PV system.

The largest part of this book is focused on the first set of models. The next sections introduce the main circuit models used for PV source simulation in ordinary operating conditions.

1.3 The Double-diode Model

The double-diode model (DDM) describes the PN junction operation through the Shockley equation, and includes series and shunt resistances to incorporate the current-dependent and the voltage-dependent loss mechanisms. It has the important feature of modeling the carrier-recombination losses in the depletion region.

The non-linear equation giving the relationship between the current and the voltage at the PV source terminals is:

$$I_{pv} = I_{ph} - I_{s1}\left[e^{\frac{(V_{pv}+I_{pv}R_s)}{\eta_1 V_t}} - 1\right] - I_{s2}\left[e^{\frac{(V_{pv}+I_{pv}R_s)}{\eta_2 V_t}} - 1\right] - \frac{V_{pv}+I_{pv}R_s}{R_h} \tag{1.1}$$

This equation can be represented in any circuit-oriented simulator by the equivalent circuit shown in Figure 1.1. I_{d1} and I_{d2} are the second and the third additive terms in (1.1).

The photoinduced current I_{ph}, the two diodes' saturation currents I_{s1} and I_{s2}, the two diodes' ideality factors η_1 and η_2, and the two resistances R_s and R_h are unknown parameters. Their values have to be identified on the basis of measurements performed by the producer or by the user, in the laboratory or in the field, on the real PV unit that is to be simulated. $V_t = \frac{kT}{q}$ is the thermal voltage of the PN junction in the PV cell, and

Figure 1.1 Equivalent circuit of the double-diode model.

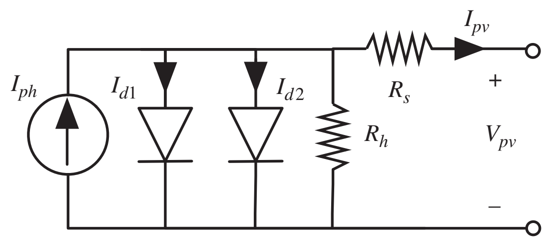

it is calculated by considering the cell temperature. The value of the second saturation current I_{s2} is three to five times higher than the first:

$$I_{s2} = \frac{T^{\frac{2}{5}}}{3.77} \cdot I_{s1} \tag{1.2}$$

Detailed expressions of the two saturation currents, including the temperature dependencies, are given in the literature [3, 4]. As for the two diodes' ideality factors, the first is often given in the literature at a value of 1 and the second at 2 [4], although their ranges of variation are $\eta_1 \in [1, 1.5]$ and $\eta_2 \in [2, 5]$ [5]. Such findings, related to the physical properties of the semiconducting material, allow a reduction in the number of parameter values to be identified on the basis of measurements performed on the specific PV source that is being modeled. This means that a small set of measurements and data, sometimes even just those given in the manufacturer's datasheet, can be used for the identification process.

Hejri et al. scaled down the number of parameter values to be identified from seven to five by fixing $\eta_1 = 1$ and $\eta_2 = 2$ [6]. This allowed them to use data available in the PV module or cell datasheet, so the problem became similar to using the SDM (see Section 2.2.1).

Besides the aforementioned one, other approaches in the literature are always based on a reduction of the number of parameter values to be identified because of the lack of seven significant sets of experimental data. For instance, the loss mechanisms might be neglected and the relationship between the two saturation currents might be used for constructing an iterative procedure converging to the optimal fitting values of the remaining parameters [7].

Such approaches, based on a preliminary symbolic manipulation of the equations, on fixing the value of some of the parameters at values taken from the literature, or on neglecting some of the terms, contrast with the adoption of an accurate model like the DDM. In the rigorous case, when all the values of the seven parameters occurring in the DDM have to be identified, fitting methods based on optimization algorithms, often based on stochastic approaches, need to be used [8]. They require large computational resources and contact with the physical problem under examination is lacking.

The DDM is able to describe accurately the behavior of thin-film cells because of its ability to give a smoother curve in the region of the maximum power point (MPP). Indeed, a high value of the ratio $\frac{I_{s2}}{I_{s1}}$ matches the typical I–V curve of thin-film cells, while $I_{s2} = 0$ gives a more abrupt transition from the constant-current to the constant-voltage branches of the I–V curve, which is much more typical of crystalline-cell technology [9]. This is confirmed by literature data and studies on crystalline-Si cells, which show that junction recombination is a mechanism that can be neglected, so that a SDM is sufficient for modeling this kind of PV cell. The usefulness of the double-diode-based modeling of crystalline cells is restricted to an improved accuracy at both high and low irradiance levels [4].

1.4 The Single-diode Model

Although it has some inaccuracies at low irradiance levels, the SDM is very often used in the literature to model crystalline-silicon-based PV generators. The recombination current is neglected; it is fixed at $I_{s2} = 0$ in (1.1) so that the corresponding equation is given by (1.3). The simplified equivalent circuit is shown in Figure 1.2.

$$I_{pv} = I_{ph} - I_s \left[e^{\frac{(V_{pv}+I_{pv}R_s)}{\eta V_t}} - 1 \right] - \frac{V_{pv} + I_{pv}R_s}{R_h} \tag{1.3}$$

Depending on the desired simulation accuracy, the SDM can be simplified further. In the literature it is often considered a lossless model; see Figure 1.3a, where both the series and the shunt resistances are neglected, the former put to zero and the latter to infinity. This choice leads to inaccuracies:

- when the numerical analysis involves very high irradiance levels, because the significant voltage drop across R_s is neglected (see Figure 1.3b)
- in mismatched conditions, because the significant current flowing into R_h in these conditions is not modeled (see Figure 1.3c).

The non-linear functions in (1.4)–(1.6) give the current–voltage relationships corresponding to the equivalent circuits shown in Figures 1.3a–c, respectively.

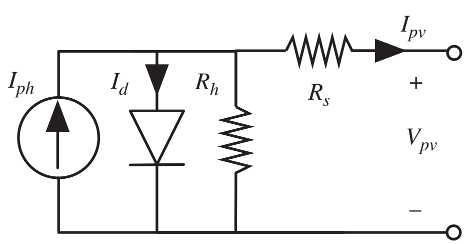

Figure 1.2 Equivalent circuit of the single-diode model.

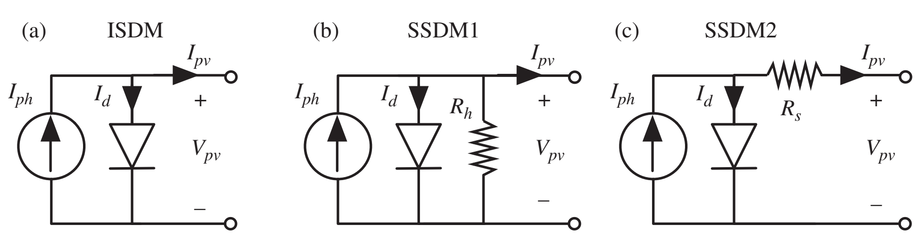

Figure 1.3 Equivalent circuits of (a) the ideal single-diode model; (b) and (c) two simplified single-diode models.

$$I_{pv} = I_{ph} - I_s \left(e^{\frac{V_{pv}}{\eta V_t}} - 1 \right) \tag{1.4}$$

$$I_{pv} = I_{ph} - I_s \left(e^{\frac{V_{pv}}{\eta V_t}} - 1 \right) - \frac{V_{pv}}{R_h} \tag{1.5}$$

$$I_{pv} = I_{ph} - I_s \left[e^{\frac{V_{pv}+I_{pv}R_s}{\eta V_t}} - 1 \right] \tag{1.6}$$

1.4.1 Effect of the SDM Parameters on the I–V Curve

Equation 1.3, or equivalently its approximate versions, allows us to know the I–V relationship for any PV source operating in homogeneous conditions. Indeed, under the assumption that all the cells are equal and subject to the same environmental conditions, the parameters (I_{ph}, I_s, η, V_t, R_s, R_h) can be scaled up or down by accounting for the number of the cells/panels connected in series to form a string, and the number of strings connected in parallel. In such conditions the voltages are multiplied by N_s, the number of the series-connected cells, and all the currents are multiplied by N_p, the number of parallel-connected strings. Consequently, the series resistance R_s and the parallel resistance R_h increase by a factor N_s and are divided by a factor N_p. The SDM parameters are scaled as follows:

$$I_{ph} = N_p \cdot I_{ph,cell} \tag{1.7}$$

$$I_s = N_p \cdot I_{s,cell} \tag{1.8}$$

$$\eta = \eta_{cell} \tag{1.9}$$

$$V_t = N_s \cdot V_{t,cell} \tag{1.10}$$

$$R_s = \frac{N_s}{N_p} \cdot R_{s,cell} \tag{1.11}$$

$$R_h = \frac{N_s}{N_p} \cdot R_{h,cell} \tag{1.12}$$

An example of the use of these scaling equations is reported in Table 1.1, where the SDM parameters of a crystalline PV panel operating in standard test conditions (STC) have been derived starting from the corresponding cell parameters. Figure 1.4 shows the corresponding I–V curve (continuous line), obtained using the scaled parameters in (1.3).

Table 1.1 Scaling up the SDM parameter for a PV panel of 36 cells in series.

Parameters	Units	Cell values	Panel values
I_{ph}	A	6.1	6.1
I_s	A	1.2172×10^{-9}	1.2172×10^{-9}
R_s	mΩ	9.2	331.2
R_p	Ω	12.7	457.2
η		1.1377	1.1377
V_t	mV	25.7	924.1

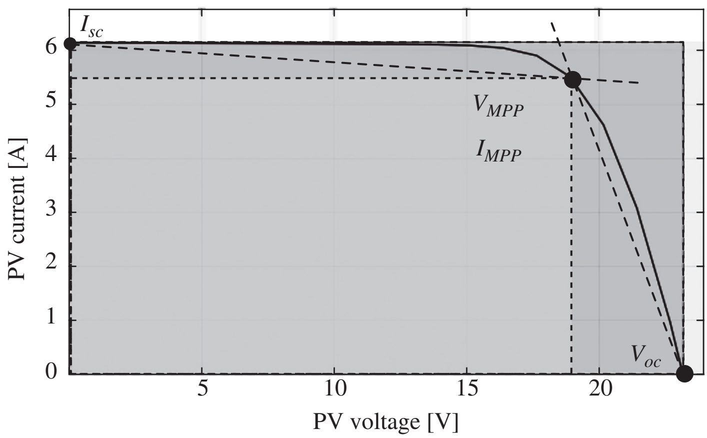

Figure 1.4 Fill factor identification on a I–V curve.

For each PV source, the three main operating points are the ones marked on the I–V curve of Figure 1.4: the short-circuit current (I_{sc}), the MPP (V_{MPP}, I_{MPP}), and the open-circuit voltage (V_{oc}). The fill factor (FF) is the basic indicator usually used for quantifying the quality of a PV panel. The FF is defined as in (1.13); it represents the ratio between the areas of the two rectangles shown in Figure 1.4. The higher the FF, the lower is the slope of the I–V curve in the region of the short-circuit current and the higher is the slope close to the open-circuit voltage.

$$FF = \frac{V_{MPP} \cdot I_{MPP}}{V_{oc} \cdot I_{sc}} \tag{1.13}$$

Figures 1.5 and 1.6 show the modification of the I–V curve due to SDM parameter variations. The photoinduced current (I_{ph}) affects mainly the vertical translation of the I–V curve, while the saturation current (I_s) and the ideality factor (η) affect the horizontal translation of the I–V curve. As will be shown in Chapter 3, such I–V curve translations are directly related to the irradiance (G) and ambient-temperature (T_a) operating conditions of the PV panel under study. The values of R_s and R_h affect mainly the slopes of the I–V curve in the regions of the open-circuit voltage and short-circuit current respectively. The variation of these two parameters is mainly related to degradation and aging, which affects the performance of the PV panel.

1.5 Models of PV Array for Circuit Simulator

From the electrical point of view, the PV source might be reproduced in any circuit simulator using linear components and a diode that represents the PN junction inside the PV cells, as shown in Figure 1.7. This representation is suitable for simulating the PV system in stationary environmental conditions because all parameters have been assumed constant. Nevertheless, in many cases it is desirable to simulate the PV source in the presence of irradiance and temperature variations, for example for testing maximum power point tracking (MPPT) algorithms. This necessitates many changes to the parameters $\overline{\mathbf{P}} = [I_{ph}, I_s, \eta, R_s, R_h]$ during the simulations on the basis of the environmental variations.

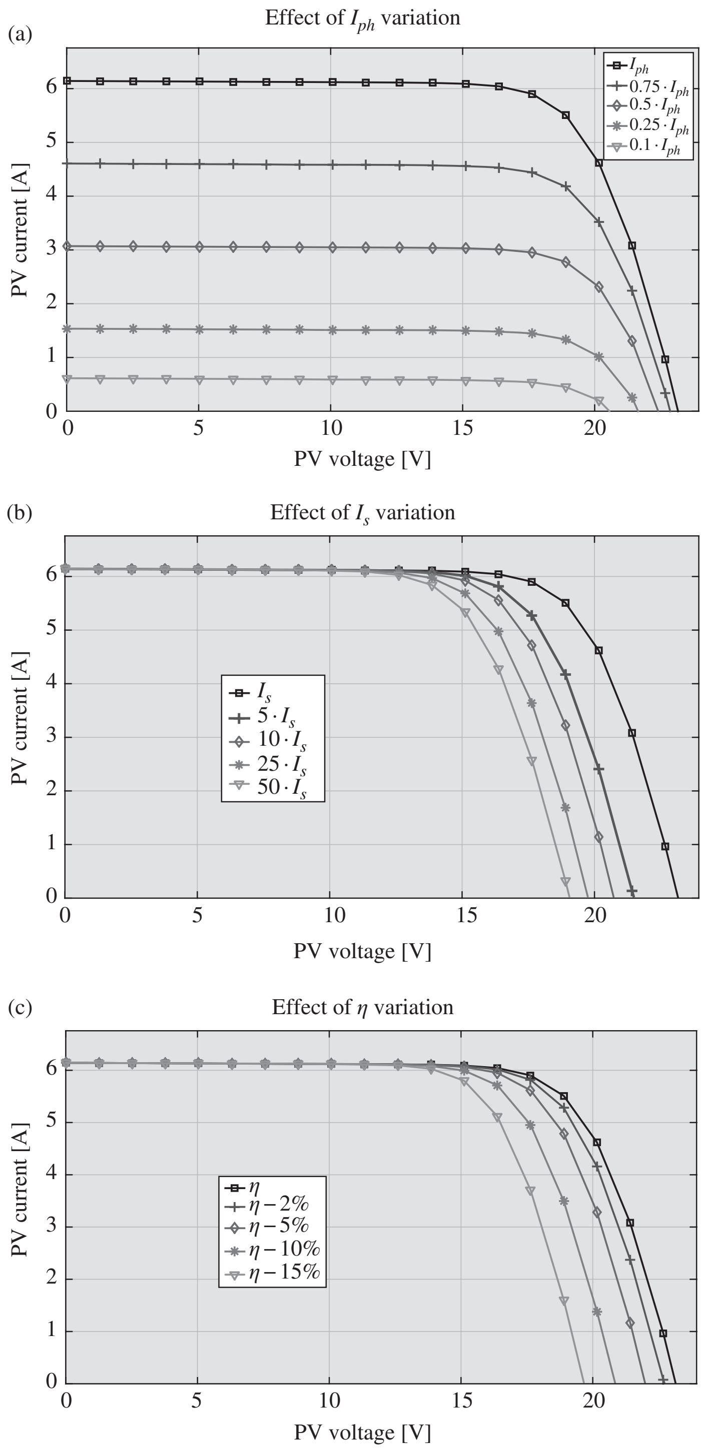

Figure 1.5 I–V curve modification due to SDM parameter variation.

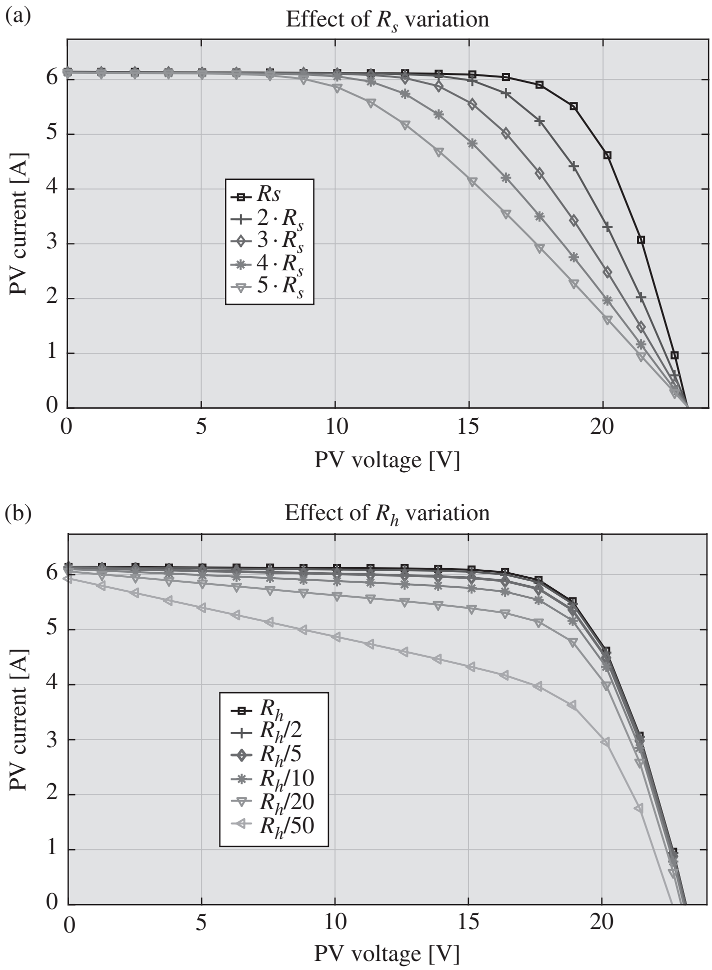

Figure 1.6 I–V curve modification due to R_s and R_h variation.

The modification of any element of $\overline{\mathbf{P}}$ during the simulation allows reproduction, with high precision, of the behavior of the PV source, improving the simulation results. Many commercial software circuit simulators have configurable embedded blocks that characterize the PV sources, and which can take into account the effects of the irradiance and temperature variations. Tools for extracting the $\overline{\mathbf{P}}$ parameters from the manufacturers' datasheet are also delivered.[1] In some cases the embedded blocks are not suitable for studying complex configurations, for example in simulations where the operating conditions are not the same for all the cells of the PV array, or simply because they are not optimized in terms of calculation speed. For these reasons the implementation of PV models developed on the basis of the guidelines given in Chapters 5 and 6 are preferable because they are more flexible and easily portable to any simulation software.

1 The reader is invited to visit, for example, the webpage at: http://powersimtech.com/solutions/renewable-energy/.

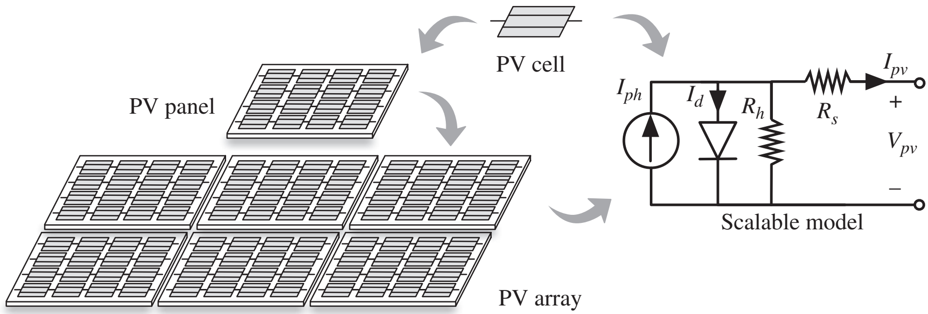

Figure 1.7 The scalable SDM can be used to model a single PV cell or a large PV field operating in homogeneous and stationary environmental conditions.

If the simulator allows implementation of mathematical equations, the PV sources can be reproduced using the scheme shown in Figure 1.8a, where the parameters η, I_{ph}, and I_s are calculated as functions of the instantaneous irradiance and temperature conditions. The parameters R_s and R_h are assumed to be constant. The voltage (V_d) across the parallel resistance R_h is measured at each simulation step, so the current (I_g) is calculated explicitly by exploiting the SDM non-linear equation, as shown in the figure. The controlled current generator is used to interface the numerical part with the electrical

Figure 1.8 PV electrical schemes based on computational blocks suitable for simulating PV fields in presence of irradiance (G) and ambient temperature (T_a) variations.

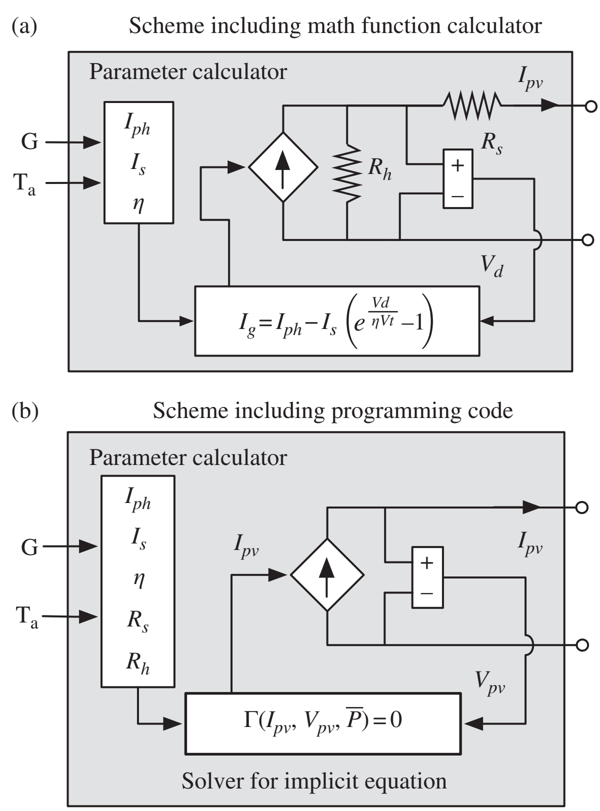

circuit connected to the PV block. Usually in short-term simulations, the temperature dependence can be neglected because it is assumed to change much more slowly with respect to the irradiance, and thus to have no impact on the fast dynamics of the whole PV system. This approach is widely used because both parameters and PV current can be calculated explicitly.

Many circuital simulators accept user-defined functional blocks (for example developed in C code), so the simulation of the PV field can be improved by using detailed models and optimized procedures. Figure 1.8b shows the complete model-based electrical scheme: the first elaboration process adapts the $\overline{\mathbf{P}}$ parameters on the basis of the instantaneous environmental conditions; the second user-defined block solves, for each simulation step, the implicit equation: $\Gamma(I_{pv}, V_{pv}, \overline{\mathbf{P}}) = 0$, derived from (1.3). The solution of the implicit equation gives the set point to the controlled current generator that provides the current at devices connected to the PV field.

Of course, if iterative procedures are used for solving the embedded blocks, the computational burden can increase significantly, making the simulation too demanding. The approaches described in the following have been selected from the literature and represent a good trade-off in terms of accuracy and elaboration speed.

1.5.1 The Single-diode Model based on the Lambert W-function

Equation (1.3) can be expressed in explicit form if the Lambert W-function is used to calculate the solution of the exponential equation; if $y = xe^x$, then $x = W(y)$. Many details and useful references about the Lambert W-function can be found in the literature [10, 11].

After some manipulations, the PV current can be expressed as function of V_{pv} and $\overline{\mathbf{P}}$ as follows:

$$I_{pv} = F\left(V_{pv}, \overline{P}\right) = \frac{R_h \cdot \left(I_{ph} + I_s\right) - V_{pv}}{R_s + R_h} - \frac{\eta \cdot V_t}{R_s} \cdot W\left(\theta_I\right) \tag{1.14}$$

where:

$$\theta_I = \frac{\left(R_h // R_s\right) \cdot I_s \cdot e^{\frac{R_h \cdot R_s \cdot \left(I_{ph} + I_s\right) + R_h \cdot V_{pv}}{\eta \cdot V_t \cdot \left(R_h + R_s\right)}}}{\eta \cdot V_t} \tag{1.15}$$

with $x // y = x \cdot y / (x + y)$.

Alternatively the PV voltage can be expressed as function of I_{pv} and $\overline{\mathbf{P}}$ as follows:

$$V_{pv} = H\left(I_{pv}, \overline{P}\right) = R_h(I_{ph} + I_s) - (R_h + R_s)I_{pv} - \eta \cdot V_t \cdot W\left(\theta_V\right) \tag{1.16}$$

where:

$$\theta_V = \frac{R_h \cdot I_s \cdot e^{\frac{R_h \cdot \left(I_{ph} + I_s - I_{pv}\right)}{\eta \cdot V_t}}}{\eta \cdot V_t} \tag{1.17}$$

The explicit equations allow the easy implementation of the PV model in any simulation environment because no iterative procedure is required to find the operating point of the PV source. The only significant effort is in the calculation of $W(\theta)$. The Lambert W-function can be decomposed into branches expressed by simpler functions, so

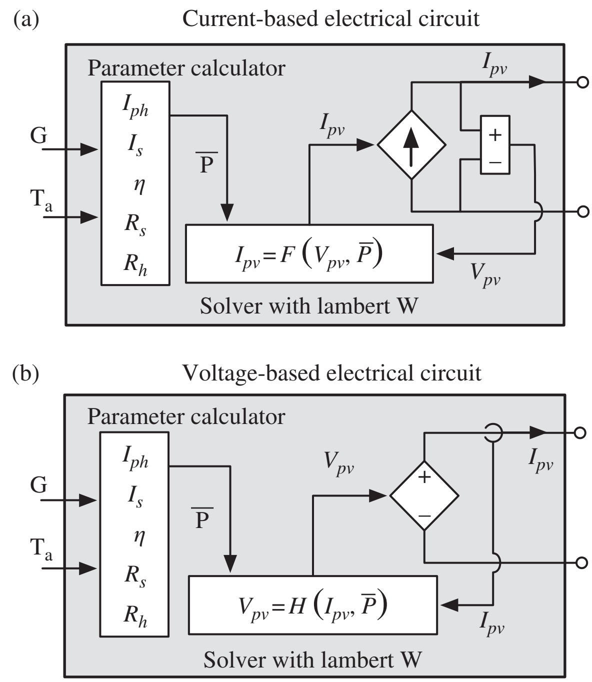

Figure 1.9 PV electrical schemes based on the Lambert W-function.

it can be implemented in any programming language [10, 11]. The schemes of Figure 1.9 show the simple blocks that might be implemented in the circuit simulator to obtain a lightweight, flexible, and reliable PV model by means of (1.14) and (1.16).

Batzelis et al. derived some approximate equations based on the Lambert W-function for calculating, in closed form, V_{MPP} and I_{MPP} too [12]:

$$V_{MPP} \simeq \frac{R_s + R_h}{R_h}\eta V_t(w-1) - R_s I_{ph}\left(1 - \frac{1}{w}\right) \tag{1.18}$$

$$I_{MPP} \simeq I_{ph}\left(1 - \frac{1}{w}\right) - \frac{\eta V_t(w-1)}{R_h} \tag{1.19}$$

where $w = W(I_{ph}e/I_s)$.

Unfortunately in non-uniform operating conditions, the PV models are not scalable and a different approach must be adopted. The extension of the methodologies shown in this chapter to non-uniform operating conditions will be outlined in Chapters 5 and 6.

1.6 PV Dynamic Models

The stationary models presented in Section 1.4, and especially the SDM, are widely adopted because they describe, by means of few components, all the main features of the PV device. They are able to reproduce with a high degree of accuracy the PV array non-linearity and the non-zero and the non-infinite slope of the I–V curve in the current and voltage generator regions, respectively. Moreover, as will be shown in Chapter 3, by adopting a suitable set of translational equations, it is also possible to simulate the PV source behavior at the desired values of irradiance and temperature.

The SDM is used, for example, for the analysis of the dynamic behavior of any MPPT algorithm implemented by means of a switching converter that processes the power produced by the PV array. As shown in Chapter 7, in real applications, it is common practice to put a capacitance in parallel with the PV array, at the input of the switching converter performing the MPPT function. This capacitance stabilizes the PV operating point by reducing the detrimental effects on the MPPT efficiency of the high-frequency ripple produced by the switching-converter operation. Unfortunately, the capacitance slows the MPPT, so that the value used comes from a compromise between MPPT dynamic performance and efficiency. The capacitance hides the dynamic behavior of the PV array, which is inherent in any diode, and thus also the behaviour of the PV source. Nousiainen et al. give a detailed dynamic analysis of the PV source [13], but major emphasis is given to the differential resistance, because the transition and the diffusion capacitances assume a negligible value with respect to the additional capacitance connected at the PV source terminals.

Figure 1.10 shows the PV dynamic model, and the two capacitive effects, C_D and C_T, that are described by the diffusion and the transition capacitances respectively. The dynamic model of the diode appearing in the SDM is completed by the differential resistance R_d [14].

These three components are non-linear, because all the three parameters R_d, C_T, and C_D are voltage-dependent [15], the last one also being dependent on the frequency [16].

By neglecting the parameters' voltage dependency, a linear model can be used to obtain the PV impedance in the desired range of frequencies. Simple algebra allows us to demonstrate that both the real and the imaginary part of the PV array impedance are frequency-dependent, not only explicitly but also through C_D. Indeed, by defining the equivalent parallel capacitance $C_p = C_T + C_D$ and resistance $R_p = R_h // R_d = R_h \cdot R_d/(R_h + R_d)$, the impedance is:

$$\begin{aligned} Z_{pv}(\omega) &= R_s + R_p // \left(-j\frac{1}{\omega C_p}\right) \\ &= \left[R_s + \frac{R_p}{1+\left(\omega R_p C_p\right)^2}\right] - j\frac{\omega R_p^2 C_p}{1+\left(\omega R_p C_p\right)^2} \end{aligned} \tag{1.20}$$

The impedance plot, in a Cartesian plane with the real and the imaginary parts of the impedance on the axes, is the best way of analyzing the frequency behavior of the PV source. Experimental results presented in the literature reveal that the typical impedance plot of the PV source is a semicircle. At a high frequency, the capacitances bypass the shunt resistance and the diode differential resistance, so that the semicircle intercepts the horizontal axis – the real part of the impedance – at a value equal to R_s.

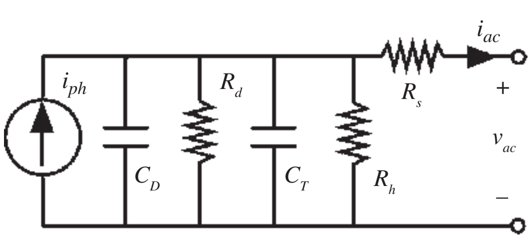

Figure 1.10 Dynamic model of the PV generator.

Meanwhile, at a very low frequency value, the capacitances behave as open circuits, so that the impedance plot intercepts the real axis at a value $R_s + R_p$. As shown by Johnson et al. for some types of PV modules [14], with cells produced with different cell technologies, this high-frequency value reaches a few hundreds of kilohertz. An example of this plot is given in Figure 1.11.

Having identified the values R_s and R_p by letting the PV source work at very high and at very low frequencies, the capacitance value C_p can be identified by analyzing the frequency behavior of the impedance. The value of C_p that minimizes the difference between the calculated impedance and the measured one is chosen [14].

This analysis can be done at any working condition of the PV generator, but values obtained in the dark are always indicated as the best in the literature. Indeed, in order to obtain the impedance plot experimentally, the PV generator must be stimulated by a sinusoidal signal (250 mV was used by Johnson et al. [14]) at different frequencies, so that so-called "impedance spectroscopy" is performed. The ratio between the phasors of the voltage and current signals at the frequency of the stimulus gives the impedance value at that frequency. The analysis in dark conditions allows avoidance of the injection of a current stimulus that must be kept considerably smaller than the average current value. The latter is the photo-induced current appearing during the day, which shows an almost linear dependency on the irradiance level.

As discussed by Chenvidhya et al. [17], in the dark, the relationship between the capacitive and the resistive effects changes significantly as a function of the PV cell's reverse or forward voltage bias. Parameters R_d, C_T, and C_D are significantly affected by the voltage bias, but also by the irradiation and temperature at which the PV generator works and by the cell's technology [18].

The capacitance remains quite low on the left-hand side of the maximum power point, the cell thus almost behaving as a current generator, but it increases dramatically when the open-circuit voltage is approached. A commonly used dependency of the capacitive effects on the operating voltage and the frequency is the following:

$$C_p\left(V,f\right) = \frac{k_1}{\left(1-\frac{V}{k_2}\right)^{0.5}} + \frac{k_3}{2\pi f} e^{\frac{V}{k_4}} \left(\sqrt{1+k_5\left(2\pi f\right)^2}-1\right)^{0.5} \tag{1.21}$$

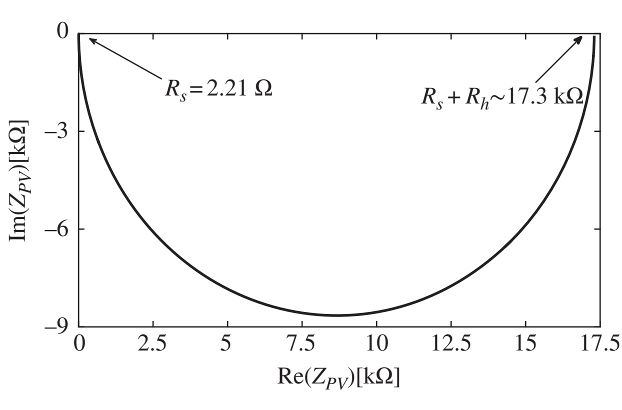

Figure 1.11 PV frequency behavior in the impedance plane; R_p = 17.3 kΩ, R_s = 2.21Ω, C_p = 2.2μF.

An extensive analysis of such dependencies has recently appeared [19]. This experimental study is especially focused on frequency analysis of a PV string during its normal operation, both in the dark and at 1000 W/m^2 conditions, and in the presence of an hot spot affecting one cell. It has become evident that both the DC impedance and the equivalent capacitance increase when an hot spot occurs. The former can be measured at few tens of hertz and the latter at some tens of kilohertz, this value being dependent on the number of cells in the PV string. The string voltage at which such measurements are made has an effect that is significantly greater than the irradiance level. The model also takes into account the parasitic series inductance of the PV string [19].

1.7 PV Small-signal Models and Dynamic-resistance Modelling

Despite the precision and the widespread adoption of the SDM, it is difficult to include its non-linear and implicit equation in control-oriented models. Moreover, to design linear and some non-linear controllers it is necessary to linearize the system model around a given operating point. That small-signal model is available in automatic tools, such as the Simulink® linearization from MATLAB®, but such a mathematic linearization can lead to small-signal models of the PV array having incorrect behavior. In the following, some small-signal approximations that have been widely adopted for PV modules are analyzed.

The first attempt to obtain a small-signal model is to expand the exponential term of (1.3) into a Taylor series, as shown in (1.22). Since the analyses performed in small-signal models around a given operating point are usually based on Laplace representations, the adopted small-signal representation of the module is linear. This constrains the Taylor series to the first two terms, which leads to the small-signal model in (1.23), where $\hat{i}_{pv_{1oT}}$ and $\hat{v}_{pv_{1oT}}$ are small-signal quantities.

$$e^{B\cdot(V_{pv}+I_{pv}\cdot R_s)} \approx 1 + B\cdot(V_{pv} + I_{pv}\cdot R_s) \tag{1.22}$$

where, $B = \frac{1}{\eta V_t}$.

$$\hat{i}_{pv_{1oT}} = \frac{R_h\cdot I_{ph}}{R_h + R_s + I_s\cdot B\cdot R_h\cdot R_s} - \frac{\left(I_s\cdot B\cdot R_h + 1\right)\cdot \hat{v}_{pv_{1oT}}}{R_h + R_s + I_s\cdot B\cdot R_h\cdot R_s} \tag{1.23}$$

Evaluating (1.23) with the parameters of the SDM provides a linear representation simple enough to develop a control-oriented small-signal model. To evaluate the precision of such a first-order Taylor approximation (1oT), the main points of the I–V (and P–V) curve must be analyzed. In particular, the predicted short-circuit current is given in (1.24), the open-circuit voltage is given in (1.25), and the MPP current and voltages are given in (1.26) and (1.27), respectively.

$$I_{sc_{1oT}} = \frac{R_h\cdot I_{ph}}{R_h + R_s + I_s\cdot B\cdot R_h\cdot R_s} \tag{1.24}$$

$$V_{oc_{1oT}} = \frac{R_h\cdot I_{ph}}{1 + I_s\cdot B\cdot R_h} \tag{1.25}$$

$$I_{MPP_{1oT}} = \frac{1}{2} \cdot \frac{R_h \cdot I_{ph}}{R_h + R_s + I_s \cdot B \cdot R_h \cdot R_s} \tag{1.26}$$

$$V_{MPP_{1oT}} = \frac{1}{2} \cdot \frac{R_h \cdot I_{ph}}{1 + I_s \cdot B \cdot R_h} \tag{1.27}$$

Figure 1.12 shows a comparison between the SDM and the 1oT approximation. The simulation shows that 1oT model accurately represents the SDM from the short-circuit current up to near the MPP, only at its left-hand side. Unfortunately, the 1oT model exhibits large errors in both the MPP current and voltage and in the prediction of the open-circuit voltage. Taking into account that the PV module operates around the MPP most of the time due to the MPPT action [20–23], this model is not suitable for designing and analyzing control systems; the MPP of the 1oT approximation is very different from the MPP of the SDM model.

However, the structure of (1.23) can be used to design electrical models representing the PV module at the MPP, where two options are addressed: a current-based circuit and a voltage-based circuit. In the first case the PV current depends on the PV voltage as in (1.28), where the term I_{sc_N} corresponds to the model short-circuit current, while the slope stands for the model admittance. This is the Norton model and its electrical scheme is presented in Figure 1.13.

$$\hat{i}_{pv_N} = I_{sc_N} - \frac{1}{R_{pv_N}} \cdot \hat{v}_{pv_N} \tag{1.28}$$

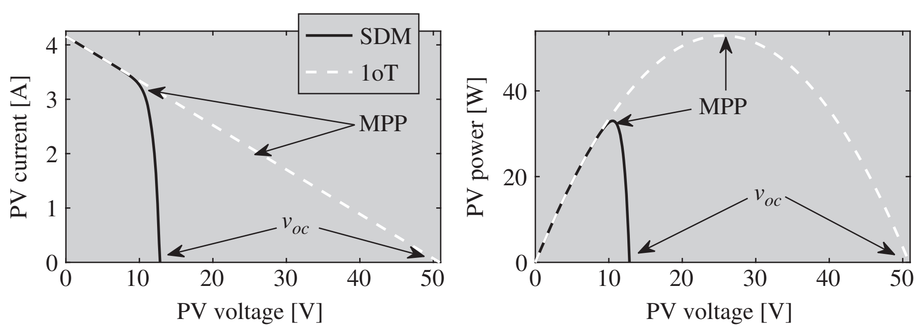

Figure 1.12 Comparison of SDM and 1oT models.

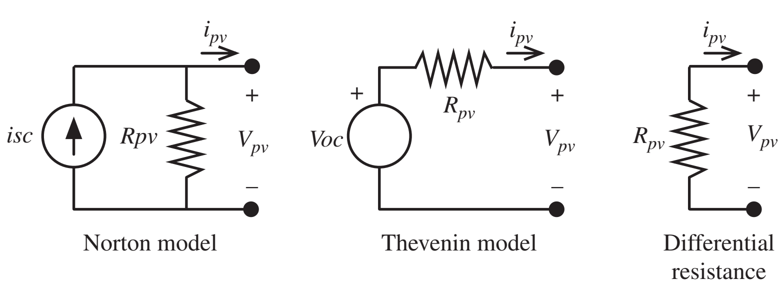

Figure 1.13 Linear small-signal models.

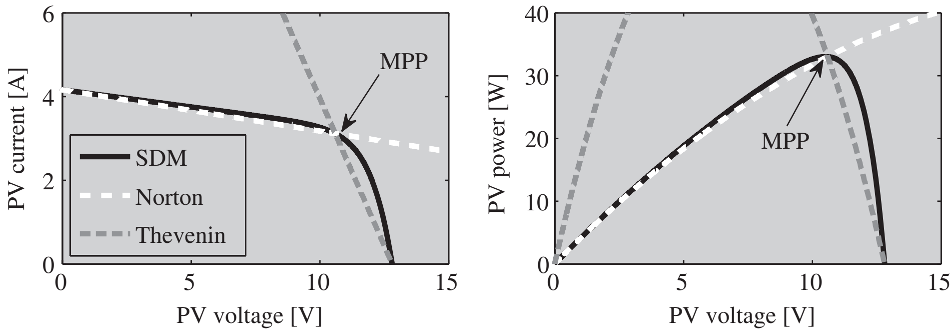

Figure 1.14 Comparison of the SDM, Norton, and Thevenin models.

The parameters I_{sc_N} and R_{pv_N} of this linear model can be calculated in different ways. A classical approach involves forcing the model to accurately reproduce both the short-circuit current I_{sc}, the MPP current I_{MPP}, and the voltage V_{MPP} using (1.29) [24].

$$I_{sc_N} = I_{sc}, \quad R_{pv_N} = \frac{V_{MPP}}{I_{sc} - I_{MPP}} \tag{1.29}$$

In the second approach – a voltage-based circuit – the PV voltage depends on the PV current as in (1.30), where the independent term V_{oc_T} corresponds to the model open-circuit voltage, while the slope stands for the model impedance R_{pv_T}. This is the Thevenin model and its electrical scheme is also presented in Figure 1.13. Classically, the model parameters ensure the accurate reproduction of both the open-circuit voltage V_{oc} and the MPP current and voltage using (1.31) [24].

$$\hat{v}_{pv_T} = V_{oc_T} - R_{pv_T} \cdot \hat{i}_{pv_T} \tag{1.30}$$

$$V_{oc_T} = V_{oc}, \quad R_{pv_T} = \frac{V_{oc} - V_{MPP}}{I_{MPP}} \tag{1.31}$$

Figure 1.14 presents a comparison of the SDM, Norton, and Thevenin approximations. This shows that both linear models accurately reproduce the MPP value, the Norton model reproduces I_{sc}, and the Thevenin model reproduces V_{oc}.

It is worth noting that neither linear model is able to reproduce the MPP power-derivative condition. Figure 1.14 shows that the MPP exhibits a power derivative equal to zero, while the Norton model predicts a positive derivative and the Thevenin model predicts a negative derivative, but small-signal models must accurately reproduce the system at the linearized operating point. Therefore, a new method to calculate the linear model parameters that accounts also for the power derivative is needed.

By solving the Norton model (1.28) for $\hat{i}_{pv_N} = I_{MPP}$, $\hat{v}_{pv_N} = V_{MPP}$, and $\frac{d\,p_{pv_N}}{d\,v_{pv_N}} = 0$, where p_{pv_N} represents the Norton power, the parameter values given in (1.32) are obtained. The Norton model, with these parameters, provides an open-circuit voltage $V_{oc_N} = 2 \cdot V_{MPP}$.

Similarly, by solving the Thevenin model of (1.30) for $\hat{i}_{pv_T} = I_{MPP}$, $\hat{v}_{pv_T} = V_{MPP}$, and $\frac{d\,p_{pv_T}}{d\,v_{pv_T}} = 0$, where p_{pv_T} represents the Thevenin power, the parameter values given in (1.33) are obtained.

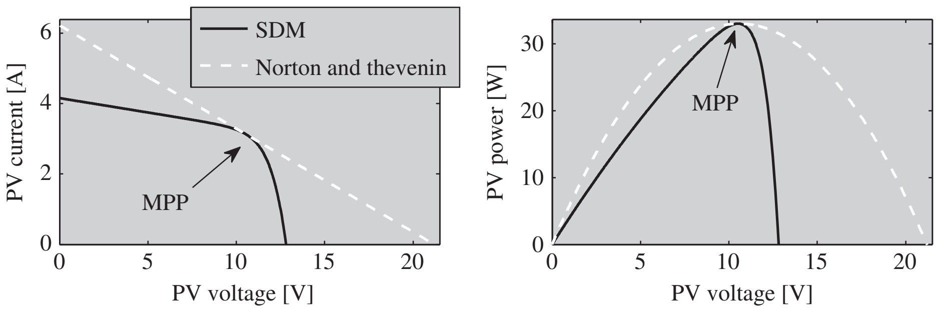

Figure 1.15 Comparison of SMD, Norton, and Thevenin models with accurate MPP approximation.

$$I_{sc_N} = 2 \cdot I_{MPP}, \quad R_{pv_N} = \frac{V_{MPP}}{I_{MPP}} \tag{1.32}$$

$$V_{oc_T} = 2 \cdot V_{MPP}, \quad R_{oc_T} = \frac{V_{MPP}}{I_{MPP}} \tag{1.33}$$

Recalling the linear circuit theory, (1.32) and (1.33) reveal that both Norton and Thevenin circuits parameterized at the MPP are equivalent, as expected. Figure 1.15 shows a comparison between the SDM and the linear small-signal models' reproduction of MPP: it can be seen that both the value and the derivative of the the power at the MPP are accurately provided by the linear model. Hence the Norton or Thevenin approximations, parameterized as in (1.32) and (1.33) respectively, are good candidates for developing a linearized model of the complete PV system, including a model of the power processing system, for control purposes.

Finally, a simpler model, named the differential resistance model, is also found in the literature [20, 21]. This model, also depicted in Figure 1.13, consists of a single impedance representing the PV module. The differential resistance magnitude is obtained from both the Norton and Thevenin models, parameterized as in (1.32) and (1.33) respectively, by nullifying the corresponding source: opening the current source in the Norton model or short-circuiting the voltage source in the Thevenin model. As expected, the differential resistance is negative, since it is derived by adopting the generator convention between the current and voltage references at the generator terminals. The differential resistance is useful for analyzing the behavior of power converters at the MPP, removing the input added to the linear system by the source of the complete linear models. Unfortunately, this characteristic shows a limitation: it is not possible to analyze the behavior of the PV system in the presence of irradiance (represented by the current source of the Norton model) or temperature (represented by the voltage source of the Thevenin model) variations.

References

1 Syafaruddin, Karatepe, E., and Hiyama, T. (2009) Artificial neural network-polar coordinated fuzzy controller based maximum power point tracking control under partially shaded conditions. *Renewable Power Generation, IET*, **3** (2), 239 –253, doi:10.1049/iet-rpg:20080065.

2 Ogliari, E., Grimaccia, F., Leva, S., and Mussetta, M. (2013) Hybrid predictive models for accurate forecasting in pv systems. *Energies*, **6** (4), 1918–1929, doi:10.3390/en6041918. URL: http://www.mdpi.com/1996-1073/6/4/1918.

3 Attivissimo, F., Di Nisio, A., Savino, M., and Spadavecchia, M. (2012) Uncertainty analysis in photovoltaic cell parameter estimation. *Instrumentation and Measurement, IEEE Transactions on*, **61** (5), 1334–1342, doi:10.1109/TIM.2012.2183429.

4 Gow, J. and Manning, C. (1999) Development of a photovoltaic array model for use in power-electronics simulation studies. *Electric Power Applications, IEE Proceedings -*, **146** (2), 193–200, doi:10.1049/ip-epa:19990116.

5 Khanna, V., Das, B., Bisht, D., Vandana, and Singh, P. (2015) A three diode model for industrial solar cells and estimation of solar cell parameters using {PSO} algorithm. *Renewable Energy*, **78**, 105–113, doi:10.1016/j.renene.2014.12.072. URL: http://www.sciencedirect.com/science/article/pii/S0960148115000063.

6 Hejri, M., Mokhtari, H., Azizian, M., Ghandhari, M., and Soder, L. (2014) On the parameter extraction of a five-parameter double-diode model of photovoltaic cells and modules. *Photovoltaics, IEEE Journal of*, **4** (3), 915–923, doi:10.1109/JPHOTOV.2014.2307161.

7 Babu, B. and Gurjar, S. (2014) A novel simplified two-diode model of photovoltaic (pv) module. *Photovoltaics, IEEE Journal of*, **4** (4), 1156–1161, doi:10.1109/JPHOTOV.2014.2316371.

8 Muhsen, D.H., Ghazali, A.B., Khatib, T., and Abed, I.A. (2015) Parameters extraction of double diode photovoltaic module's model based on hybrid evolutionary algorithm. *Energy Conversion and Management*, **105**, 552–561, doi:10.1016/j.enconman.2015.08.023. URL: http://www.sciencedirect.com/science/article/pii/S0196890415007694.

9 Miceli, R., Orioli, A., and Gangi, A.D. (2015) A procedure to calculate the i-v characteristics of thin-film photovoltaic modules using an explicit rational form. *Applied Energy*, **155**, 613–628, doi:10.1016/j.apenergy.2015.06.037. URL: http://www.sciencedirect.com/science/article/pii/S0306261915007953.

10 Weisstein, E. (2008) Lambert w-function. *A Wolfram Web Resource. http://mathworld.wolfram.com/LambertW-Function.html*.

11 Corless, R., Gonnet, G., Hare, D., Jeffrey, D., and Knuth, D. (1996) On the lambertw function. *Advances in Computational Mathematics*, **5** (1), 329–359, doi:10.1007/BF02124750.

12 Batzelis, E., Kampitsis, G., Papathanassiou, S., and Manias, S. (2015) Direct mpp calculation in terms of the single-diode pv model parameters. *Energy Conversion, IEEE Transactions on*, **30** (1), 226–236, doi:10.1109/TEC.2014.2356017.

13 Nousiainen, L., Puukko, J., Mäki, A., Messo, T., Huusari, J., Jokipii, J., Viinamäki, J., Lobera, D., Valkealahti, S., and Suntio, T. (2013) Photovoltaic generator as an input source for power electronic converters. *Power Electronics, IEEE Transactions on*, **28** (6), 3028–3038, doi:10.1109/TPEL.2012.2209899.

14 Johnson, J., Schoenwald, D., Kuszmaul, S., and Strauch, J. (2011) Creating dynamic equivalent pv circuit models with impedance spectroscopy for arc-fault modeling. *SANDIA Report*, **SAND2011-4247**.

15 Kumar, R., Suresh, M.S., and Nagaraju, J. (2006) Effect of solar array capacitance on the performance of switching shunt voltage regulator. *Power Electronics, IEEE Transactions on*, **21** (2), 543–548, doi:10.1109/TPEL.2005.869779.

16 Thongpron, J., Kirtikara, K., and Jivacate, C. (2006) A method for the determination of dynamic resistance of photovoltaic modules under illumination. *Solar Energy Materials and Solar Cells*, **90** (18 19), 3078–3084, doi:10.1016/j.solmat.2006.06.029. URL: http://www.sciencedirect.com/science/article/pii/S0927024806002200, 14th International Photovoltaic Science and Engineering Conference 14th International Photovoltaic Science and Engineering Conference.

17 Chenvidhya, D., Kirtikara, K., and Jivacate, C. (2005) {PV} module dynamic impedance and its voltage and frequency dependencies. *Solar Energy Materials and Solar Cells*, **86** (2), 243–251, doi:10.1016/j.solmat.2004.07.005. URL: http://www.sciencedirect.com/science/article/pii/S0927024804002910.

18 Kumar, R.A., Suresh, M., and Nagaraju, J. (2004) Gaas/ge solar cell {AC} parameters under illumination. *Solar Energy*, **76** (4), 417–421, doi:10.1016/j.solener.2003.10.004. URL: http://www.sciencedirect.com/science/article/pii/S0038092X03004237.

19 Kim, K., Seo, G.S., Cho, B.H., and Krein, P. (2015) Photovoltaic hot spot detection for solar panel substrings using ac parameter characterization. *Power Electronics, IEEE Transactions on*, **PP** (99), 1–1, doi:10.1109/TPEL.2015.2417548.

20 Femia, N., Petrone, G., Spagnuolo, G., and Vitelli, M. (2005) Optimization of perturb and observe maximum power point tracking method. *IEEE Transactions on Power Electronics*, **20** (4), 963–973.

21 Femia, N., Petrone, G., Spagnuolo, G., and Vitelli, M. (2009) A technique for improving p&o mppt performances of double-stage grid-connected photovoltaic systems. *IEEE Transactions on Industrial Electronics*, **56** (11), 4473–4482.

22 Bianconi, E., Calvente, J., Giral, R., Mamarelis, E., Petrone, G., Ramos-Paja, C.A., Spagnuolo, G., and Vitelli, M. (2013) Perturb and observe mppt algorithm with a current controller based on the sliding mode. *International Journal of Electrical Power & Energy Systems*, **44** (1), 346–356.

23 Bianconi, E., Calvente, J., Giral, R., Mamarelis, E., Petrone, G., Ramos-Paja, C., Spagnuolo, G., and Vitelli, M. (2013) A fast current-based mppt technique employing sliding mode control. *IEEE Transactions on Industrial Electronics*, **60** (3), 1168–1178.

24 Trejos, A., Gonzalez, D., and Ramos-Paja, C.A. (2012) Modeling of step-up grid-connected photovoltaic systems for control purposes. *Energies*, **5** (6), 1900–1926.